Achieving Pseudo-Ductile Behavior of Carbon Fiber Reinforced Polymer Composites via Interfacial Engineering

Gábor Szebényi,* Balázs Magyar, and Tibor Czigany

This article presents an investigation of the properties of interfacial engineered carbon fiber (CF) reinforced polymer (CFRP) composites. Poly(ε-caprolactone) (PCL) is used as an interface engineering/interlayer material to modify the interfacial shear strength (IFSS) between the phases, with which it is aimed to increase the pseudo-ductility of CFRPs. A stable crack propagation behavior can be achieved through interfacial engineering due to the locally weakened connection between the resin and the fiber reinforcement. Various grid patterns of PCL interfacial additive are designed, and 3D printed on the unidirectional (UD) CF (UDCF) surfaces by fused deposition modeling (FDM) and the UDCF is infiltrated with an amine-cured epoxy (EP). The resulting composites are subjected to mechanical tests. In each case, the PCL-rich interphase increases ductile pseudo-behavior, and the type of grid affects the mechanical response.

1. Introduction

High-performance composites with carbon fiber (CF) reinforced epoxy (EP) matrix are widely used for low-weight, high-strength demanding applications. As a result, more attention is paid to these materials and their potential.[1] Composite materials are often compared with metals and their properties. In terms of strength, nearly, the same characteristics can be achieved with lower weight. The substitution of metals may be possible in specific applications, but the most considerable disadvantage of composite systems is the tendency for sudden, catastrophic failure at specific loads, where metals are ductile, and so, their failure is not catastrophic. Ductility shows the ability of the material to withstand high load without fracture, through irreversible

Dr. G. Szebényi, B. Magyar, Prof. T. Czigany
Department of Polymer Engineering
Faculty of Mechanical Engineering
Budapest University of Technology and Economics
Muegyetem rkp. 3, H-1111 Budapest, Hungary
E-mail: szebenyi@pt.bme.hu

Prof. T. Czigany
MTA–BME Research Group for Composite Science and Technology
Muegyetem rkp. 3, H-1111 Budapest, Hungary

The ORCID identification number(s) for the author(s) of this article can be found under https://doi.org/10.1002/adem.202000822.

plastic deformation. This plastic deformation absorbs more energy than the preceding elastic deformation phase.[2] In the case of CF reinforced polymer (CFRP) matrix composites, there is no plastic deformation—failure often appears suddenly with a high energy release rate. Therefore, classical ductility (as in the case of metals), which requires plastic deformation, cannot be interpreted. In plastic deformation, a non-linear connection between the load and the deformation appears. Due to the non-linear section, the energy absorption capacity increases. However, plastic stress-deformation behavior can be achieved without plastic deformation itself with a stable damage mode. This form of damage behavior is so-called pseudo-ductility in the case of CFRPs, because the metal-like stress–strain relationship with progressive, non-linear response can be achieved without plastic deformation.[3] Due to the pseudo-ductile behavior, the absorbed energy during failure can be increased, and the ductility index (DI) can be improved. The DI is an essential value in this regard, showing the type of failure.[4]

Interlayer modification techniques have already shown their potential to solve the problem mentioned earlier. One of the interlayer techniques is the addition of a fiber layer, which can have high strain (HS) compared with the low-strain (LS) CF layers. This results in a more gradual failure compared with that of neat CFRPs, which display brittle behavior. This technique uses hybridization, where the matrix has at least two types of fiber reinforcements. By hybridization, the properties of the phases appear together, showing synergistic effects. In tension, the LS fibers fail first, which does not lead to catastrophic failure (i.e., CFRP) and is followed by the failure of the HS fibers. As a result, gradual failure occurs. At failure, different kinds of damage appear in the reinforcing structures. The LS reinforcements fragment first, multiple cracks develop, followed by the delamination of the two phases ending with the failure of the HS phase at a higher deformation level.[5–7]

Several studies used this method with different types of HS layers. Zhang et al.[8] conducted falling dart impact and three-point bending tests on glass fiber (GF)/CF hybrid and pure CF and GF composites with EP resin. They observed that the different types of CF/GF layups had a significant effect on the absorbed energy. Composites, which had more GF layers or were only reinforced with GF layers, had more energy absorption capacity compared with the neat CF reference composites, but they showed worse strength values. Sena-Cruz and co-workers[6] experimented with different layups to observe the hybridization

**ADVANCED
SCIENCE NEWS**

www.advancedsciencenews.com

**ADVANCED
ENGINEERING
MATERIALS**

www.aem-journal.com

effect. They found that the hybridization effect depends on many factors, i.e., the vol% of the LS fibers and also the non-dimensional stiffness parameter (END). Czél and Wisnom[5] investigated CF/EP (EP resin) and GF/EP thin-ply hybrid composites. During the failure of the laminates, they observed that pseudo-ductile behavior appeared as a result of the stable pullout and fragmentation of the carbon layers. However, many other reinforcements can be used instead of GF, such as aramid,[9] highly oriented polyethylene (HOPE),[10] or even steel fibers[11] for this purpose. Quan et al.[11] used steel fibers as an interlayer. They found that Young's modulus remained the same while Mode-I fracture energy increased significantly. Sohn and Hu[12] used chopped aramid fiber layers between CF layers. They showed that the aramid fibers improved Mode-II fracture toughness with a more pronounced crack growth section in the failure process.

Another interlayer technique is, where a ductile, mostly a thermoplastic polymeric layer that is placed between CF layers. The ductile interlayer has greater deformation and damping capacity; thus, brittle crack propagation is hindered. Wang et al.[13] used poly(ethylene-co-methyl acrylate) (EMA) and poly(ethylene-co-methacrylic acid) (EMAA) as a thin interlayer ply. With the specific plies, interlaminar fracture toughness improved significantly with a drop of shear strength compared with the untreated reference samples measured in a double cantilever beam (DCB) test. The thermoplastic layer also provides self-healing. They also healed the composite laminate at 150 °C. As a result of healing, they found that the inspected composite was able to withstand additional loads with a significant drop in shear strength and also in interlaminar fracture toughness. Rezadoust and co-workers[14] used electrospun polyvinylbutyral (PVB) nano-web as a thermoplastic interlayer. They observed that the nanofibers increased Mode-I and Mode-II fracture toughness of the composite in DCB and end-notched flexure (ENF) tests; thus, the nanofibers inhibited crack propagation. Nanowebs thicker than 30 μm resulted in significantly worse mechanical properties.

The interlayer films have great potential; however, they can increase the weight of the composites, and there is also the above-mentioned shear strength loss.[15] Locally placed interlayers could be an answer[16–19] to these problems. With this method, only locally interlayered zones are created, as opposed to the previously presented thermoplastic ply method, where the whole surface was covered. These local zones do not considerably increase the weight of the composite, and strength does not decrease significantly. In our previous paper,[17] we showed the feasibility of using a fused deposition modeling (FDM) printed interlayer, which delayed final failure. With the printed poly(ε-caprolactone) (PCL), locally weakened interfacial adhesion can be created within the matrix and the fibrous reinforcement. Due to the weakened connection, the cracks did not spread to the reinforcement, resulting in local damage. The interfacial material was soluble in the EP resin; thus, it did not create a new interphase. Zhang at al.[18] used inkjet printing of thermoplastic polymers as a local interlayer. For the printing process, they used a poly(methyl methacrylate) (PMMA) solution. They found that only 0.025 vol% interlayer additive increased interlaminar fracture toughness with minimal weight gain. Islam and Prabhakar[19] used polylactic acid (PLA) with FDM to place the interlayer onto the surface of reinforcement. They printed straight lines along the width of the specimens. As a result,

interlaminar shear strength increased in short beam shear (SBS) tests. The printed zones increased the energy absorption capability of the composite laminates during fracture. The authors also analyzed the effect of the printing parameters on the final mechanical properties of the composite laminates. They found that the bonding strength of the printed material is critical in terms of crack propagation.

The present research aims to investigate the positive results of interfacial engineering further and examine the effect of various printed interlayer grid layouts. Pseudo-ductile behavior can be traced back to the more favorable properties of the interlayers; however, the quality of the interfacial connection is also an important factor. In most research so far, additional phases have been used that did not dissolve in the matrix. Thus, these interlayers can also serve as starting points for cracks. We used a soluble thermoplastic material, PCL as local interlayer with FDM, and analyzed the effect of PCL on the interfacial shear strength (IFSS) with a microdroplet test. This test is critical in determining whether pseudo-ductile behavior appeared due to locally weakened interfacial zones. With the locally weakened IFSS, stable crack propagation can be achieved through the formation of independent crack initiation points. During the damage process, the composite laminate could absorb more energy with the formation of micro-delaminations instead of fiber breakages. We examined the effect of the temperature to ensure proper dissolution of the PCL on the interface. Also, the effect of the distribution of the interfacial material on the mechanical and pseudo-ductile properties was investigated with different interlayer grid layouts. It is a further objective of the present work to determine whether the various grids of local interfacial material could influence the mechanical properties of the composites.

2. Experimental Section

2.1. Materials

We used the IPOX ER 1010 (IPOX Chemicals Kft., Budapest, Hungary) DGEBA-based EP resin as the matrix of the composite laminates, with the IPOX MH 3124 amine-based curing agent. The mixing weight ratio was 100:35, according to the producer's recommendation. Curing this EP at room temperature yields a glass transition temperature of 80 °C. Fiber reinforcement was PX35FBUD0300 (Zoltek Zrt., Nyergesújfalu, Hungary) unidirectional (UD) carbon weave (309 g m^{-2} surface weight), consisting of Panex35 50k roving. For the 3D printed interface, we selected eMorph175N05 (Shenzhen Esun Industrial Co. Ltd., Shenzhen, China) PCL filament. We chose PCL, because it is soluble in the matrix, easier to process than other thermoplastic additives due to its lower melting temperature, and because it is a biomaterial, so it is not harmful to the environment, unlike many high-performance additives. The diameter of the filament was 1.75 mm (melting temperature, $T_m = 80$ °C, glass transition temperature, $T_g = -60$ °C, and print temperature: >80 °C).

2.2. Grid Layouts

The basic idea is that the modified interface between the matrix and the reinforcement can create locally weakened zones, which
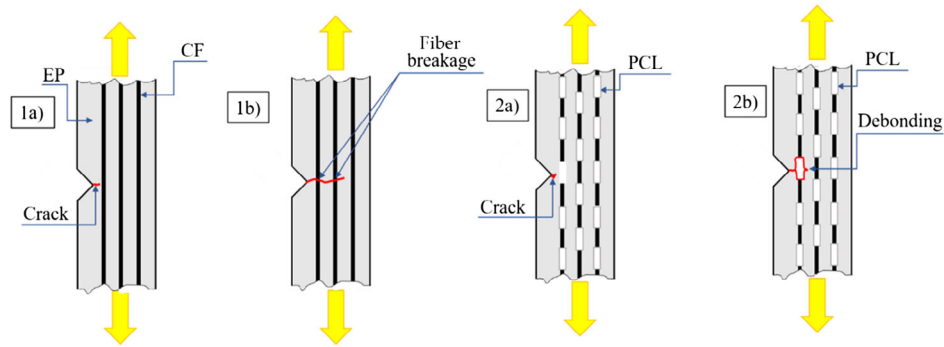
Figure 1. Crack propagation in a CFRP laminate. 1a) Crack initiation. 1b) Crack propagation causes fiber breakage due to the good IFSS. 2a) Crack initiation at the modified IFSS composite. 2b) Interfacial engineered case where the cracks do not spread to the fibers, causing local damage.

can be used to make crack propagation more secure and controllable **(Figure 1)**. During crack propagation, assuming a good interface between the phases, the crack may extend to the fiber reinforcement. This can lead to fiber breakage, which results in an increased load on to the surrounding elements. The overload of the surrounding areas can lead to a rapid spread of the existing crack, to the surrounding fibers, which could also cause more fiber breakages. This can trigger brittle failure with a sudden, high energy release (Figure 1(1b)). The modified zones, on the other hand, have the task of delaying the breakage of fibers and slowing down the propagation of cracks, creating localized damage. Because of the modified zones, the composite has a higher energy absorption capacity (Figure 1(2b)). In the event of an overload, failure will not occur immediately.

In our experiments, we investigated the effect of different grid layouts on mechanical properties. We had previously demonstrated the beneficial results of using a grid on the surface of the CF layer; therefore, we wanted to investigate what different grids can achieve.[17] For the grids, we created 3D models in

SolidWorks. The 2D grid layouts are shown in **Figure 2**. We tailored these grids to observe whether there is a difference between them in enhancing pseudo-ductility. In our previous publication,[17] we used a parallel grid; we used this as a reference. We created regularly positioned zones at 45° to the fibers. In the case of the edge-effect grid, we created more concentrated zones in the proximity of the supports used for the three-point bending tests and less concentrated zones where stress concentration is lower. We expected failure to occur in the concentrated zones. We created a diagonal grid, where the propagating crack can pass through several weaker adhesion zones; thereby, the probability of local delamination was increased. In the combined layout, we concentrated zones further away from the clamping and support, and the grids in the middle were dashed, so essentially more independent zones were created. With the grids, we created several locally weakened adhesion zones. As a result, we were able to determine whether the failure occurred in the treated or in the untreated zones. We printed equal amounts of PCL onto the surface of the CF. The surface filling ratio was 10%.
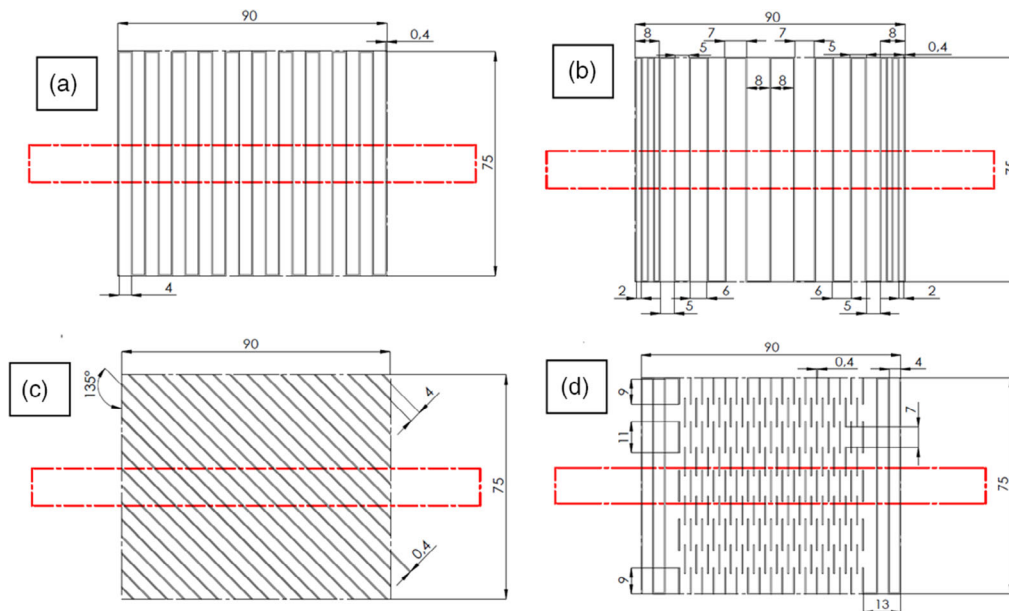
Figure 2. Different grid layouts with the position of the specimen (red contour) (the dimensions are in mm). a) Parallel. b) Edge effect. c) Diagonal. d) Combined.

**ADVANCED
SCIENCE NEWS**

www.advancedsciencenews.com

**ADVANCED
ENGINEERING
MATERIALS**

www.aem-journal.com

We put the previously cut reinforcement layers on the print bed of the 3D printer with the fiber direction parallel to the main movement axis of the print head and printed on one side of the weave. Each grid consisted of a single filament with a different spacing. The print head was heated to 180 °C, and the temperature of the print bed was 40 °C. The PCL material was printed on one surface of the UDCF with a CraftBot Plus 3D printer. **Figure 3** shows the printing process.

Figure 4 shows the exact layup of the composite. We printed on five layers, and then covered the stack with an untreated CF layer. During curing, the weaker adhesion zone is also formed on the non-printed side of each layer, as they come into contact with each other. This is even easier to achieve if the non-crimp fabric layers are pressed together before laminating. In the magnified part, the desired macrostructure is shown. Where the PCL comes into contact with the reinforcement CF, interfacial adhesion is weakened. Also, in this area, the matrix is more ductile because of the toughening effect of the PCL additive. The weight ratio of the PCL in the composite laminate was around 0.5%. With the interfacial engineering material, the thickness of the composite increased as well, from 3.1 ± 0.2 mm (reference) to 3.4 ± 0.23 mm.
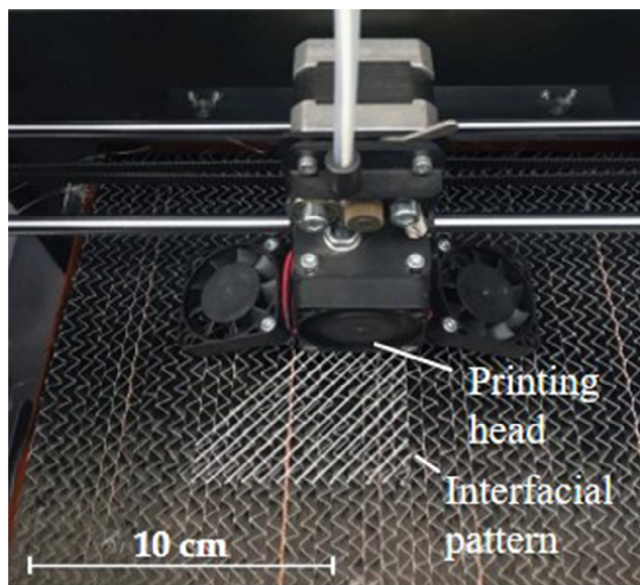

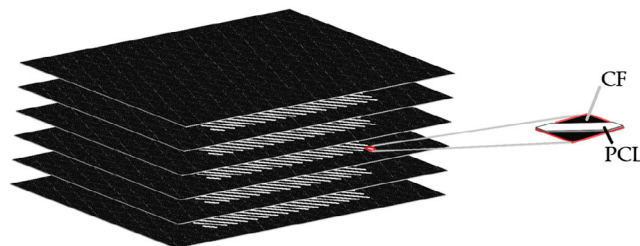**Figure 3.** Printing the grid on the UDCF weave.

Figure 4. Exploded view of the composite laminate, five interlayers with printed diagonal zones, and the desired macrostructure (magnified section).

2.3. Preparation of the Composites

The six-layer UD composites were created by hand layup followed by vacuum pressing. The reinforcing layers were impregnated with the EP resin with peel plies on both the top and bottom layers. This eased removal from the polyethylene terephthalate film that covered the glass sheet mold. A vacuum bag was built over the laminate to provide uniform pressure and high fiber content. A vacuum of 0.5 bar was applied for 20 min at room temperature, and then, the samples were cured in a drying oven at 80 °C for 1 h. In the case of interlaminar-gridded samples, five gridded layers and one neat layer were laid up in a way that the grids were present in all the interlayers. Under these conditions, PCL is only partly dissolved in the EP. The laminate thickness of the reference composite was 3.1 mm; the thickness of the CF/EP composites with the PCL printed grids was 3.4 mm. The specimens were cut from the laminates with a Mutronic Diadisc diamond disc saw according to the standard specifications.
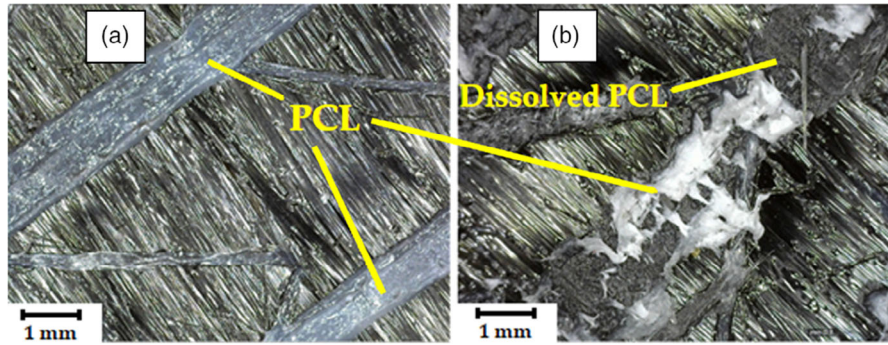
3. Results and Discussion

3.1. The Effect of Curing on the Grid

We used different curing methods in the production of the composites to determine the appropriate curing temperature for the dissolution of the PCL. We also observed how the grid changes during dissolution. During preparation, we printed the PCL on only one UDCF layer; then, we impregnated it with the EP resin. For this microscopy examination, we printed 1 mm wide grids on the CF layer. We used two curing temperatures. For reference, we used room temperature ($\approx$30 °C), whereas for the second examination, we used a drying oven at 80 °C for 1 h. To determine the changes in dimensions, we used an AM4113ZT Dino Lite Premier optical microscope. **Figure 5**a represents the results without heat treatment. Here, the dimensions have not changed, and dissolution was not completed either. The measured line width was 1.14 ± 0.22 mm, close to that in the computer-aided design model. The use of the drying oven did not change the dimensions significantly; line width was 1.21 ± 0.23 mm. Dissolution was clearly visible in this case. The matt zones in the same direction as the printed grid show the dissolved PCL.

At room temperature, the contour of the PCL grid is clearly visible after curing. Even though the temperature was above melting temperature, the PCL did not spread on the CF surface, because the EP resin essentially encapsulated the material, and crosslinking also took place within 1 h. The PCL dissolved in the EP matrix but did not spread on the surface of the CF (so the grid was intact) in the case of high-temperature curing.

3.2. Microdroplet Test

We performed microdroplet tests to determine the shear strength of the interface between the pure or the modified resin and the CF, to investigate how the presence of PCL modifies adhesion. A test speed was 2 mm min^{-1}, and the distance of the pulling blades was 30 µm. Thus, the CF was able to move

**ADVANCED
SCIENCE NEWS**

www.advancedsciencenews.com

**ADVANCED
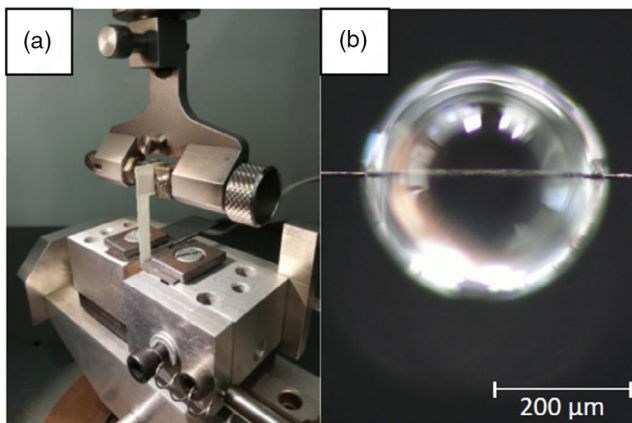ENGINEERING
MATERIALS**

www.aem-journal.com

Figure 5. 50× magnified pictures from a cured laminate a) cured at room temperature and b) cured in a drying oven at 80 °C.

between the blades on a slate, and the blades were able to load the droplets. For the test, a drop of the matrix material was dripped on a single CF, and the drops were supported by the blades during the tests. The fiber embedded in the drop was pulled by a tensile tester. If the maximum force is known, the diameter of the fiber and the length of the embedded section, the shear stress of the interface, and the critical length of the fiber can also be calculated (Equation (1)).
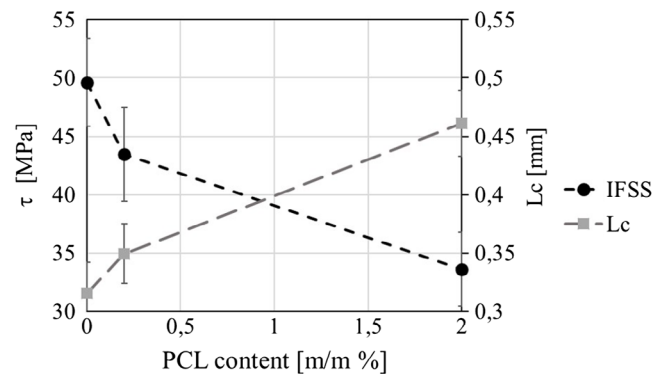
$$\tau = F_C / (\pi \times d_f \times L_c) \tag{1}$$

where τ is the IFSS, F_C is the maximal measured force, d_f is the diameter of a single fiber, and L_c is the length of the embedded fiber. The dimensions of the drop and the fiber were determined with an optical microscope (Olympus BX51M). We used pure EP resin as reference and various PCL mass concentrations in EP resin (0.2 and 2 m m^{-1}%) to determine the effect of the additive on IFSS. The droplets applied to the single fibers were cured at 80 °C for 1 h (**Figure 6**).

The IFSS decreased significantly when the m m^{-1}% of the PCL in the EP matrix was increased. Thus, interfacial adhesion also weakened significantly at the PCL concentration of 2 m m^{-1}% (**Figure 7**). To determinate the significance of the results, we used the analysis of variance method with a confidence interval of 95%. In the printed zones, the surface modifier

Figure 7. Microdroplet test results.

material is present in a much higher concentration, so in terms of adhesion, the PCL will be the dominant material. Thus, other adhesion conditions appear in gridded zones, which could lead to pseudo-ductile behavior. As a result, PCL is capable of locally modifying the IFSS, helping the formation of small controlled zones for delamination.

Due to the weakened zones, crack propagation can change. When a crack comes into contact with a modified zone, propagation can be slowed down. The crack will not spread to the fibers; thus, there is no fiber breakage, but local delamination may appear (results of ten tests with each m m^{-1}%).

3.3. Three-Point Bending Test

For the three-point bending tests, we used a Zwick Z020 computer-controlled universal tester. The tests were performed according to EN ISO 14125. There is a difference between the stress values (**Table 1** and **Figure 8**) of the specimens: a 100 MPa fall in the maximal bending stress of the edge-effect grid. The other modified samples behaved in nearly the same way as the reference samples. The maximum stress is also reached earlier by the modified samples, but with a longer ductile plateau; the final failure is reached at much higher deformation. The different behaviors can be attributed to the different design of the grids. In the case of the edge-effect grid, there is a significant decrease in strength. The reason for this can be that the adhesion rate is significantly reduced at two points locally.

Figure 6. Microdroplet test. a) Measurement arrangement. b) EP drop on a single CF.

Table 1. Bending test results.

	E [GPa]	σ_m [MPa]	ε_m [%]	σ_b [MPa]	ε_b [%]	SAE [MJ m^{-3}]	DI [—]
Reference	36.8 ± 3.6	556.7 ± 27.0	1.8 ± 0.2	340.2 ± 101.0	2.0 ± 0.1	6.7 ± 0.3	0.81 ± 0.13
Parallel	36.0 ± 2.5	529.4 ± 28.6	1.8 ± 0.2	304.4 ± 90.4	2.3 ± 0.1	7.3 ± 0.3	0.72 ± 0.14
Edge effect	32.0 ± 2.7	405.6 ± 17.4	1.7 ± 0.3	267.0 ± 135.1	2.6 ± 0.2	7.1 ± 0.3	0.65 ± 0.15
Diagonal	35.9 ± 4.1	465.4 ± 39.2	1.5 ± 0.2	233.2 ± 136.3	2.4 ± 0.1	7.7 ± 0.3	0.54 ± 0.11
Combined	30.6 ± 3.7	451.6 ± 44.1	1.6 ± 0.2	167.8 ± 62.4	2.6 ± 0.4	7.3 ± 0.4	0.66 ± 0.14
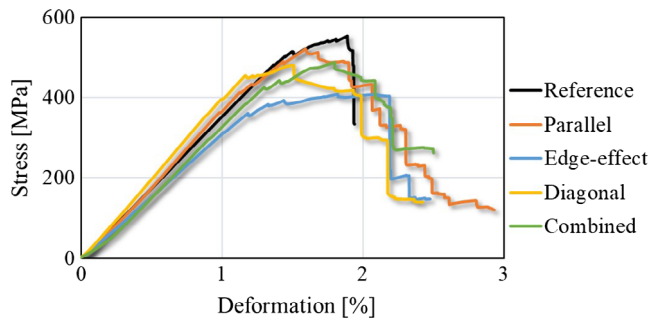
Figure 8. Specific three-point bending test curves.

Therefore, the cracks can be concentrated at these points. The different grids enhance ductility in different degrees; the diagonal and combined grids have several distinct weakened adhesion regions, which makes cracks more likely to collide with these zones.

In the case of the reference specimens, after the maximum stress (σ_m) was reached, the specimens did not show any resistance; they broke suddenly. In the case of the modified samples, after this limit was reached, failure was prolonged, and deformation at the maximal stress (ε_m) also increased. To determine damage progress, we investigated the bending curves around the maximal stress (Figure 8). There are many steps before maximal stress is reached in the case of the reference specimens, which indicates a higher energy release during failure at each step. Failure happens with significant drops in the stress level with high energy release. Therefore, these specimens cannot take considerable deformation after reaching maximum stress (Table 1). In the case of the modified samples, the curve is much flatter, which indicates damage at several local points. The specimens with a modified grid were significantly more deformable; final failure appeared at higher deformation (ε_b). The area under the curve shows the specific absorbed energy (SAE) during the bending test. In the case of modified samples, the absorbed energy increased significantly. The SAE value was approximated with the Riemann integral (Equation (2)).

$$\int_a^b f(x)\mathrm{d}x = \lim_{n \to \infty} \sum_{i=1}^n f(\xi_i)(x_i - x_{i-1}) \qquad (2)$$

where $f(x)$ is the stress-deformation function, a is the initial point (0), b is the end point of the curve in which failure occurs,

x is the deformation, and ξ is the stress for the given deformation. The area under the curve has two major parts: crack initiation energy and crack propagation energy. From those two energies, the DI can be calculated. A decrease in DI indicates that the ductility of the specimens was enhanced. A DI close to 1 means that failure was rigid, and a DI close to 0 indicates ductile damage. Total absorbed energy was calculated with Equation (3).

$$E_T = E_{CI} + E_{CP} \qquad (3)$$

where E_T is the total absorbed energy, and E_{CI} is the crack initiation energy, whereas E_{CP} is the crack propagation energy. E_{CI} is the absorbed energy until maximal stress is reached, and E_{CP} is the energy beyond that. From these, the DI can be calculated (Equation (4)).

$$DI = E_{CI}/E_T \qquad (4)$$

The DI also shows that interfacial engineering has a significant effect on the ductile behavior of the material. Differences in DI were more pronounced. Especially in the case of the diagonal gridded specimens, the DI dropped by 32% compared with the reference specimens. After reaching maximum stress, the modified specimens were capable of further gradual deformation. The reason for this is controlled crack propagation. In the modified samples, many independent elements were damaged, the failure of which did not cause the whole system to fail. However, in the case of the reference samples, the occurrence of damage had a significant effect on the reliability of the system. After reaching maximum stress, high energy release can be observed in these samples.

4. Conclusion

Our goal was to increase the pseudo-ductility of CF reinforced EP matrix composites. We investigated the possibility of using a designable interface between the resin and the fibers to improve ductility. We created a designed interface grid by FDM printing to modify interfacial adhesion locally.

We determined the effect of PCL on the IFSS with microdroplet tests. We found that with increased PCL content, the IFSS significantly changed. With altered connection, we created designable zones to achieve pseudo-ductile behavior.

We created various grids and examined their effect, and used equal surface filling in every grid. Our conclusion is that the different grid layouts had a significant effect on mechanical and

especially on pseudo-ductile behavior. The different behavior is due to the type of load, its direction, and the direction of crack propagation. In the case of the parallel, edge effect, and combined grid, the layout was perpendicular to the orientation of the reinforcement. Each grid element was shorter in these cases, compared with the diagonal pattern, and the tests showed that the cracks can collide with these zones with higher probability.

In our forthcoming research, we will continue the investigation of the effects of designed interlaminar grids on the ductility of composite structures, with a particular focus on the effect of surface filling ratio and dynamic properties.

Conflict of Interest

The authors declare no conflict of interest.

[1] A. Asadi, M. R. Abusrea, K. Arakawa, J. Colton, K. Kalaitzidou, *Express Polym. Lett.* **2018**, *12*, 781.

[2] J. Case, L. Chilver, C. T. F. Ross, *Strength of Materials and Structures*, 4th ed. (Eds: J. Case, L. Chilver, C. T. F. Ross), Butterworth-Heinemann, London **1999**, p. 12.

[3] J. D. Fuller, M. R. Wisnom, *Compos. A: Appl. Sci. Manuf.* **2018**, *107*, 31.

[4] R. José, J. Tarpani, O. Maluf, M. Cristina, M. C. Gatti, *Mater. Res.* **2009**, *12*, 395.

[5] G. Czél, M. R. Wisnom, *Compos. A: Appl. Sci. Manuf.* **2013**, *52*, 23.

[6] F. Ribeiro, J. Sena-Cruz, F. G. Branco, E. Júlio, *Construct. Building Mater.* **2018**, *171*, 871.

[7] Y. Swolfs, Y. Geboes, L. Gorbatikh, S. T. Pinho, *Compos. A: Appl. Sci. Manuf.* **2017**, *103*, 1.

[8] C. Zhang, Y. Rao, Z. Li, W. Li, *Materials* **2018**, *11*, 2472.

[9] S. Stefanidis, Y. W. Mai, B. Cotterell, *J. Mater. Sci. Lett.* **1985**, *4*, 1033.

[10] M. Cao, Y. Zhao, B. H. Gu, B. Z. Sun, T. E. Tay, *Compos. Struct. 211* **2019**, 175.

[11] D. Quan, S. Flynn, M. Artuso, N. Murphy, C. Rouge, A. Ivanković, *Compos. Struct.* **2019**, *210*, 49.

[12] M.-S. Sohn, X.-Z. Hu, *Compos. Sci. Technol.* **1994**, *52*, 439.

[13] C. H. Wang, K. Sidhu, T. Yang, J. Zhang, R. Shanks, *Compos. A: Appl. Sci. Manuf.* **2012**, *43*, 512.

[14] H. Ipakchi, A. M. Rezadoust, M. Esfandeh, M. Rezaei, *Thin-Walled Struct.* **2020**, *151*, 106724.

[15] Y. Zhang, J. Stringer, A. Hodzic, P. Smith, *J. Compos. Mater.* **2017**, *52*, 1567.

[16] V. Damodaran, A. G. Castellanos, M. Milostan, P. Prabhakar, *Mater. Des.* **2018**, *157*, 60.

[17] G. Szebényi, T. Czigány, B. Magyar, J. Karger-Kocsis, *Concept Feasibility* **2017**, *11*, 525.

[18] Y. Zhang, J. Stringer, R. Grainger, P. J. Smith, A. Hodzic, *Phys. Status Solidi (RRL)* **2014**, *8*, 56.

[19] M. S. Islam, P. Prabhakar, *Mater. Des.* **2017**, *133*, 332.